

Ordering in Two-Dimensional Dipolar Mixtures

Julia Fornleitner,^{*,†} Federica Lo Verso,^{‡,⊥} Gerhard Kahl,[†] and Christos N. Likos^{§,||}

[†]Center for Computational Materials Science (CMS) and Institut für Theoretische Physik, Technische Universität Wien, Vienna, Austria, [‡]Chimie Analytique et Biophysico-chimie de l'Environnement (CABE), Université de Genève - Sciences II, Genève 4, Switzerland, [§]Institut für Theoretische Physik II: Weiche Materie, Heinrich-Heine-Universität Düsseldorf, Düsseldorf, Germany, and ^{||}The Erwin Schrödinger International Institute for Mathematical Physics (ESI), Vienna, Austria. [⊥]Current affiliation: Institut für Physik, Johannes-Gutenberg-Universität Mainz, Mainz, Germany

Received February 3, 2009. Revised Manuscript Received March 6, 2009

Two-dimensional dipolar mixtures consisting of spherical particles with unequal susceptibilities are shown to order to an enormous variety of crystalline structures, whose geometry can be tuned by the stoichiometry of the compound, the susceptibility ratio, as well as the density. Our results are based on the application of genetic algorithms, which allow for an efficient and unbiased search over the parameter space. Structures that are practically degenerate energetically are discovered at various parameter combinations. Implications on the ability to tune the phononic spectra of such composite materials are discussed.

1. Introduction

Soft matter offers ideal and yet unprecedented possibilities to stabilize arrangements of colloidal particles in monolayers. Confined either at the interface of suitably chosen substances (such as air, water, or oil) or between parallel glass plates that are separated by a sufficiently small distance from each other, colloidal particles are forced to stay confined on a single layer. The properties of the system and thus the arrangement of the particles can conveniently be influenced via several routes: by an appropriate choice of the confining walls or of the properties of the confining substances, by an application of external fields, or by a suitably chosen architecture of the colloidal particles themselves. Thus we have a sheer unlimited freedom to investigate the self-assembly scenarios of such systems at hand. In addition, the size of typical colloidal particles (ranging from 1 nm to 1 μ m) allows for direct observation of the particles' positions in simple optical microscopes. These ideal experimental conditions to investigate the properties of colloidal monolayers are in striking contrast to the rather restricted situation encountered in hard matter systems, where atomic monolayers have to be grown on structured substrates, whose structural and electronic properties are predefined and thus impose considerable influence on the properties of the layers. Additionally, only indirect methods of observation, such as various scattering techniques, are available for atomic systems.

This contribution is dedicated to detailed investigations of ordered monolayer configurations in two specific soft matter systems. Both of them have been studied previously: In the first system, polystyrene particles are trapped on an air/water interface. Experiments have been performed for the one-component system^{1,2} and computer simulations have been carried out for the same setup, this time for both the one-component case³ and a binary mixture with particles having different size.⁴ Following arguments put forward by Sun et al.,³ there is strong evidence that the interaction is an induced dipole–dipole interaction. The other

system has been studied in experiment;^{5,6} it is a binary mixture of superparamagnetic particles, floating on a pendant water droplet and exposed to an external magnetic field perpendicular to the interface. The field forces the dipoles to orient parallel to the field and thus the interaction is a pure dipole–dipole potential. A more detailed consideration reveals that the two systems are closely related: the interparticle potentials derived by Sun et al.³ for the first system display a $1/r^3$ behavior from intermediate distances onward, a behavior that is characteristic for the interaction of the latter system. Thus we expect that, up to moderate number densities, both systems will display identical ordered particle arrangements. Only at high densities, where the particles start to feel the difference in the short-range behavior of the potential, differences in the structural properties of the two systems are to be expected.

Both experiments and simulations performed on these two systems have provided clear indications of an overwhelmingly rich wealth of ordered equilibrium structures. However, because of the well-known limitations of both approaches, such as finite ensemble size, fluctuations in the local densities, and so forth, neither of the two approaches is able to provide a comprehensive set of ordered equilibrium structures. It is also not possible to explore the sequence of ordered particle arrangements as the system parameters—i.e., density, composition, particle size ratio, susceptibilities—vary in a systematic way. In contrast, a purely theoretical approach is able to fill this gap, and this is the aim of the present contribution: at a given state point, the ordered particle arrangement for either of these two systems is obtained by minimizing the thermodynamic potential that characterizes the system. However, such a minimum has to be found in a highly complex, rugged search space so that nearly all of the commonly used optimization strategies are bound to fail. In this contribution, we use ideas of genetic algorithms (GAs),⁷ to identify the configurations of minimal energy. The very general and broadly applicable approach of GAs uses elements of natural evolution,

*Corresponding author. E-mail: fornleitner@cmt.tuwien.ac.at.

(1) Aveyard, R.; Clint, J.; Nees, D.; Paunov, V. *Langmuir* **2000**, *16*, 1969–1979.

(2) Aveyard, R.; Clint, J.; Nees, D.; Quirke, N. *Langmuir* **2000**, *16*, 8820–8828.

(3) Sun, J.; Stirner, T. *Langmuir* **2001**, *17*, 3103–3108.

(4) Stirner, T.; Sun, J. *Langmuir* **2005**, *21*, 6636–6641.

(5) Hoffmann, N.; Ebert, F.; Likos, C. N.; Löwen, H.; Maret, G. *Phys. Rev. Lett.* **2006**, *97*, 078301.

(6) Ebert, F.; Keim, P.; Maret, G. *Eur. Phys. J.* **2008**, *26*, 161.

(7) Holland, J. *Adaptation in Natural and Artificial Systems*; The University of Michigan Press: Ann Arbor, 1975.

such as mutation, mating, and recombination. The choice of this search strategy is justified by the fact that it has proven to be a highly successful, efficient, and reliable optimization tool in a meanwhile broad variety of soft matter systems.^{8–14} The strength and reliability of GAs in such problems probably lies in the fact that GAs basically search among all possible equilibrium structures, i.e., in the entire search space, without putting a bias on the search.

With this powerful tool at hand, we are indeed able to identify the ordered equilibrium structures for our two systems. Performing investigations at zero temperature, an overwhelmingly rich variety of complex particle arrangements has been obtained. Now that a systematic variation of the system parameters is within reach, we provide an overview of the ordered equilibrium structures that the system can attain. Even more, the complex sequences of structure which emerge as we vary composition and size ratio can be interpreted as a very complex competition between the large and small particles, based on energetic and topological arguments: in their effort to either “squeeze” into the vacancies of the host lattice of the larger particles, or, if these void spaces are not sufficiently large, to modify this lattice, the smaller particles develop a remarkable amount of originality to arrange in a host of patterns, ranging from dimers, trimers, and over cup-like oligomeric arrangements to ring-patterns or lanes.

The dipolar system at hand allows us to investigate and obtain insight into the role played by the *interactions* in bringing up nontrivial ordering on binary compounds. The dipolar interactions at hand have the additional properties of being long-range, thus local “packing rules” do not offer the way of approach for such systems. This is in stark contrast to the well-studied case of binary hard-disk mixtures,¹⁵ for which geometric constraints and local packing effects dictate the stability of the resulting structures. A critical comparison between the variety of resulting arrangements will be presented in Sec. 4. The fact that some of the particle arrangements of dipolar mixtures are very exotic, low-symmetry structures points out that GA-based search strategies are indeed superior to conventional approaches for this particular problem.

The paper is organized as follows: The systems, models and interaction potentials are presented and physically discussed in section 2. In section 3 we present a detailed account of the search strategy, i.e., the aforementioned GA, employed to the current problem, whereas in section 4 we show and discuss our results. In section 5 we summarize and draw our conclusions.

2. Model and System

Our theoretical investigations are based on two experimental setups that, at first sight, have nothing in common. In the first setup, labeled by a superscript I, sulfate latex particles are floating at an oil–water interface, thus guaranteeing a two-dimensional geometry. By the use of a Langmuir trough, the particle density is controlled.^{1,2} Although the complex mechanism of the interparticle potential could not be fully revealed, the interactions are

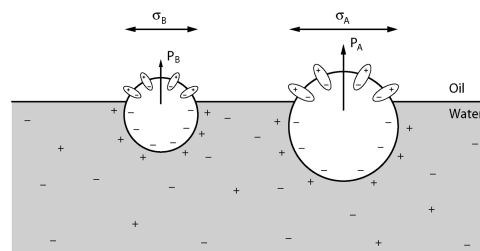


Figure 1. Schematic representation of system I (inspired by Stirner and Sun⁴): Two polystyrene particles of different size float at an oil–water interface. They interact via dipole moments P_A and P_B , that are the vector sum of the surface charge dipoles sitting at the interface of the particle with the oil.

believed to have their origin in the formation of surface charge dipoles on the particle’s interface with the oil phase. These considerations, which are supported by the fact that all experimental findings could be reproduced in simulations based on these effective interactions, are outlined in the following:^{3,16} On contact with water, hydrophilic sulfate head groups on the particles’ surfaces dissociate, and surface charge dipoles are formed. Since the particles are covered by a thin water film when poured into the setup, dipole charges are found on the entire surface of the particle. In the aqueous phase however, the interaction of these dipoles is shielded as a result of the small Debye length in water, so that the effective dipole moment is given as the vector sum of all the surface charge dipoles sitting at the particles’ interface with the oil phase (see Figure 1). This complex scenario has been cast in a theoretical model.³ For a binary mixture of particles of different radius (R_A and R_B), the resulting potentials for two particles, carrying dipole moments P_i and P_j and separated by a distance r , thus read as⁴

$$\Phi_{ij}^I(r) = \begin{cases} \infty & r \leq (R_i + R_j) \\ \frac{P_i P_j}{16\pi\epsilon R_i R_j r} \ln \left[\frac{r^2 - (R_i - R_j)^2}{r^2 - (R_i + R_j)^2} \right] & r > (R_i + R_j) \end{cases} \quad i, j = A, B \quad (1)$$

where ϵ denotes the dielectric constant of water. If we assume

$$P_i = \alpha R_i^{(n+2)/2} \quad (2)$$

set $z = R_B/R_A < 1$ and $x = r/\sigma_A$, and, in addition, extract a suitable common prefactor $E_I = \alpha^2 R_A^n / (16\pi\epsilon)$ acting as an energy scale, we arrive at

$$\Phi_{AA}^I(x) = E_I \frac{1}{x} \ln \left[\frac{x^2}{x^2 - 1} \right] \quad \text{for } x \geq 1 \quad (3)$$

$$\Phi_{BB}^I(x) = E_I \frac{z^n}{x} \ln \left[\frac{x^2}{x^2 - z^2} \right] \quad \text{for } x \geq z \quad (4)$$

$$\Phi_{AB}^I(x) = E_I \frac{z^{n/2}}{x} \ln \left[\frac{4x^2 - (1-z)^2}{4x^2 - (1+z)^2} \right] \quad \text{for } x \geq (1+z)/2 \quad (5)$$

(8) Gottwald, D.; Likos, C. N.; Kahl, G.; Löwen, H. *Phys. Rev. Lett.* **2004**, *92*, 068301.

(9) Gottwald, D.; Likos, C. N.; Kahl, G.; Löwen, H. *J. Chem. Phys.* **2005**, *122*, 074903.

(10) Gottwald, D.; Kahl, G.; Likos, C. N. *J. Chem. Phys.* **2005**, *122*, 204503-1.

(11) Mladek, B. M.; Gottwald, D.; Kahl, G.; Neumann, M.; Likos, C. N. *Phys. Rev. Lett.* **2006**, *96*, 045701.

(12) Pauschenwein, G. J.; Kahl, G. *Soft Matter* **2008**, *4*, 1396–1399.

(13) Fornleitner, J.; Kahl, G. *Europhys. Lett.* **2008**, *82*, 18001.

(14) Pauschenwein, G. J.; Kahl, G. *J. Chem. Phys.* **2008**, *129*, 174107.

(15) Likos, C. N.; Henley, C. L. *Philos. Mag. B* **1993**, *68*, 85–113.

(16) Sun, Y.; Stirner, T. *J. Chem. Phys.* **2004**, *121*, 4292–4296.

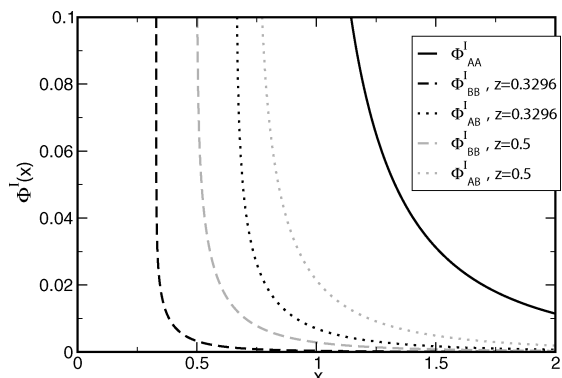


Figure 2. Interaction potentials $\Phi_{ij}^I(x)$ for two different values of the particle size ratio z : $z = 0.3296$ (black dashed lines) and $z = 0.5$ (gray dashed lines).

From these formulations of the $\Phi_{ij}^I(x)$, it is obvious that the two potential parameters z and n influence the form of the interaction potential in the following way: taking $\Phi_{AA}^I(x)$ for reference, since it is independent of z or n , a lowering of the value of z decreases the range of the repulsive tails of $\Phi_{BB}^I(x)$ and $\Phi_{AB}^I(x)$ and weakens their strengths, as the smaller particles have a smaller dipolar moment (see Figure 2). The exponent n , on the other hand, makes the potential softer with decreasing n (see Figure 3). In the other experimental setup (denoted by the superscript II), a binary mixture of superparamagnetic colloids is confined in a pending water droplet, trapping the particles in a two-dimensional geometry^{5,6,17,18} (see Figure 4). A strong magnetic field \mathbf{B} , applied perpendicular to the surface, induces dipolar moments $\mathbf{M}_i = \chi_i \mathbf{B}$, $i = A, B$ in the particles, and thus leads to the following pair interaction:

$$\Phi_{ij}^{II}(x) = E_{II} \frac{m_i m_j}{x^3}, \quad i, j = A, B \quad (6)$$

with $E_{II} = \mu_0 \chi_A^2 \mathbf{B}^2 / (32\pi R_A^3)$, if we use the larger susceptibility χ_A as a scale and $m_i = \chi_i / \chi_A \leq 1$, $i = A, B$, in the above equation.

The intimate relation between the two sets of potentials becomes obvious if we expand the $\Phi_{ij}^I(x)$ in a Taylor series, retaining the first term:

$$\Phi_{ij}^I(x) \sim \frac{(z_i z_j)^{(n+2)/2}}{x^3} + \mathcal{O}(x^{-5}) \quad (7)$$

with $z_{ij} = 1$ or z as $i, j = A$ or B , which represents exactly the interactions in a binary mixture of perfect dipoles. The corresponding equivalence relation between the particle size ratio z and the susceptibility ratio m is given by

$$m_i \leftrightarrow z_i^{(n+2)/2}, \quad i = A, B$$

In a double-logarithmic plot of the potentials 3–5, it is clearly visible, that the typical power-law behavior of the ideal dipole–dipole interaction is reached for $x > 1.5$ (see Figure 5). At low and intermediate densities, where the particles are separated sufficiently far from each other, the two sets of potentials, 3–5 and 6, are therefore practically identical, leading to the same ordered particle arrangements. At higher densities, however, the Taylor expansion (eq 7) is not valid and differences in the equilibrium structures of the two systems will occur.

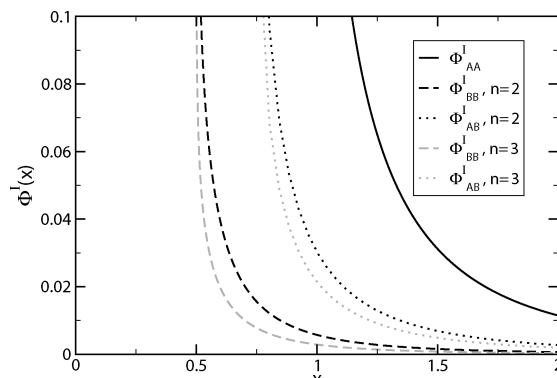


Figure 3. Interaction potentials $\Phi_{ij}^I(x)$ for two different values of the exponent n : $n = 2$ (black dashed lines) and $n = 3$ (gray dashed lines).

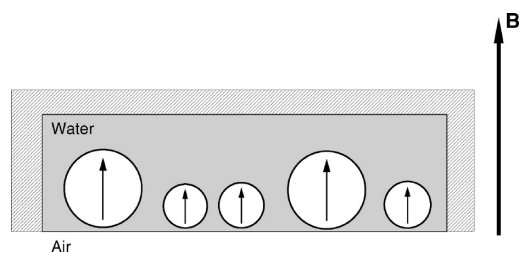


Figure 4. Schematic representation of system II (inspired by Ebert et al.⁶): Superparamagnetic, colloidal particles of two different sizes are trapped on the interface of a pending water droplet. An external magnetic field \mathbf{B} induces magnetic moments in the colloids.

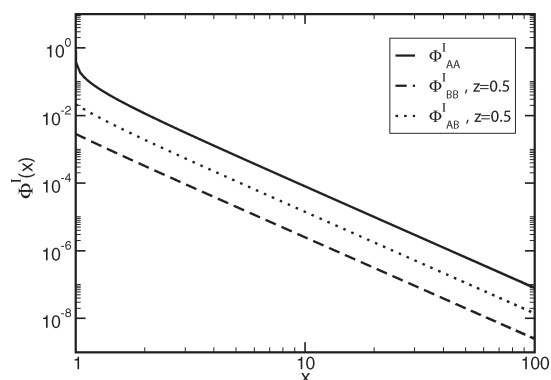


Figure 5. Double logarithmic plots of the $\Phi_{ij}^I(x)$ for $z = 0.5$, demonstrating their $\sim x^{-3}$ power-law dependence for large and intermediate distances.

Furthermore, we would like to point out that for intermediate and large particle separations, one of the two potential parameters used to describe system I becomes superfluous in 7, as, e.g., a change in the exponent, $n \rightarrow \tilde{n}$, can always be translated to a change in the particle size ratio,

$$n \rightarrow \tilde{n} \leftrightarrow z \rightarrow \tilde{z} = z^{(n+2)/\tilde{n}+2} \quad (8)$$

In what follows, we have employed an exponent of $n = 3$ in all calculations.

3. Genetic Algorithms

Our strategy to find the candidate structures for the ordered particle arrangements is based on ideas of GAs.⁷ The general method as well as the specific implementation for a

(17) Hoffmann, N.; Likos, C. N.; Löwen, H. *J. Phys.: Condens. Matter* **2006**, *18*, 10193.

(18) Assoud, L.; Messina, R.; Löwen, H. *Europhys. Lett.* **2007**, *80*, 48001.

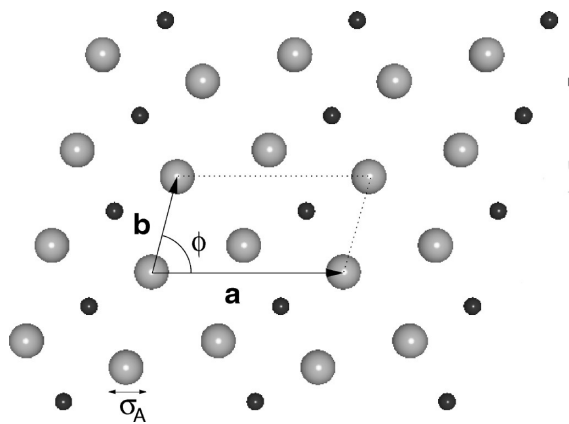


Figure 6. Ordered two-dimensional lattice structure of a binary mixture. An arbitrary choice of lattice vectors is indicated. The diameter of the larger particle species, σ_A , is chosen as a length scale.

two-dimensional system are briefly described by Gottwald et al.¹⁰ and Fornleitner and Kahl.¹³ In this section we focus on the details of the implementation of our GA-based approach for a binary, two-dimensional system introduced by Fornleitner et al.¹⁹

Before starting to explain the main outline of a GA-search strategy as we use it, two terms have to be clarified: (i) An individual \mathcal{I} —which is a string of genes, encoded in the chosen, binary alphabet—represents one candidate solution to the problem at hand (i.e., a possible lattice structure) (see Figure 7 for an example). (ii) The set of individuals at a given iteration cycle of the algorithm is called a *population* or *generation*. We start the algorithm with a randomly chosen generation, the individuals of which consist of completely arbitrary sequences of genes. In the next step, all individuals are assigned a fitness value $f(\mathcal{I})$, which in our case depends on the lattice sum of the crystal encoded in the individual. $f(\mathcal{I})$ is a measure for the quality of the solution represented by individual \mathcal{I} in the sense that a higher fitness value $f(\mathcal{I})$ characterizes a better solution. Then, pairs of individuals (“parents”) are chosen according to their fitness for reproduction. Using crossover mechanisms of different levels of sophistication, new individuals (“children”) are generated, forming the next population of the algorithm. We point out that the exact method of selecting and reproducing individuals determines the way in which the search space is sampled and has thus significant influence on the performance of the algorithm. After recombination, mutation takes place. Individuals are selected for mutation at random with a probability p_m and some of the genes are arbitrarily changed in the chosen individual(s). In this way lost genetic material can be reintroduced, and inbreeding is avoided. The cycle of evaluation—selection—reproduction—mutation is repeated until a termination condition is met. The best individual of each generation is stored and the overall best individual of *all* populations then represents the result of the GA.

The basic principles outlined above have to be adapted to the specific problem, i.e., to finding minimum energy configurations (MECs) for two-dimensional binary mixtures: First, we have to find a convenient way to translate the physical solutions, i.e. the crystal structures, to strings of genes; second, a suitable fitness function has to be chosen to evaluate the quality of the individuals; and, third, we have to determine suitable recombination and mutation processes that guarantee a high performance of our algorithm. Essentially, we use the same lattice parametrization as

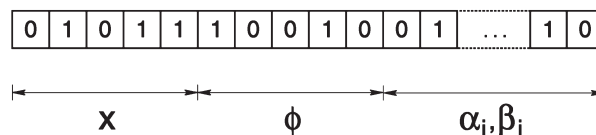


Figure 7. Parameters (x , ϕ , α_i , β_i) that characterize a possible lattice structure encoded in the individual.

the one presented by Gottwald et al.;¹⁰ however, since we deal with binary mixtures, all structures are now, by definition, nonprimitive lattices, i.e., crystal lattices with at least two basis particles. Each structure is described via two lattice vectors \mathbf{a} and \mathbf{b} , which span the unit-cell and via s vectors $\mathbf{B}_1, \dots, \mathbf{B}_s$ indicating the positions of the s particles that form the basis. We are free to choose $|\mathbf{a}| = a \geq b = |\mathbf{b}|$, and we assume that \mathbf{a} is parallel to the x -axis. Thus we can parametrize \mathbf{a} and \mathbf{b} via

$$\mathbf{a} = a(1, 0), \quad \mathbf{b} = a(x \cos \phi, x \sin \phi) \quad (9)$$

with

$$x = \frac{|\mathbf{b}|}{|\mathbf{a}|}, \quad \tilde{\phi} = \frac{2}{\pi} \phi \quad (10)$$

as independent parameters; note that $0 < x \leq 1$ and $0 < \tilde{\phi} \leq 1$.

The length scale a is uniquely determined by the particle density $\eta\sigma_A^2$ of the system

$$\frac{a}{\sigma} = \sqrt{\frac{s}{\eta\sigma^2 x \sin \phi}} \quad (11)$$

and thus fixes the absolute size of the lattice. The diameter of the larger particle species σ_A is taken as a length scale in this parametrization (see Figure 6).

The positions of the s basis particles are given as a linear combination of the lattice vectors,

$$\mathbf{B}_i = \alpha_i \mathbf{a} + \beta_i \mathbf{b} \quad i = 1, \dots, s \quad (12)$$

with $\mathbf{B}_1 = (0, 0)$ and $\alpha_i, \beta_i \in (0, 1)$. The first n_A basis particles belong to species A and the remaining $n_B = s - n_A$ particles to species B. In this way, every possible lattice is characterized by $[2 + 2(s - 1)]$ parameters, i.e., $(x, \tilde{\phi}, \alpha_2, \beta_2, \dots, \alpha_s, \beta_s)$, all of them lying in the range $(0, 1)$.

With this parametrization in mind, we have to decide on how to encode these parameters in an individual \mathcal{I} . Since we want to use the binary alphabet for the genes, we have to translate the real valued parameters to binary numbers. To this end we first map the real valued parameter to an integer:

$$I_p = p(2^{n_p} - 1) + 1 \quad (13)$$

where p is the real valued parameter, and I_p its integer representation. n_p is the number of bits used to encode the parameter and thus gives the numerical accuracy of the encoding process. We then arrange the binary representations of the parameters to form an individual \mathcal{I} , so that the first n_x bits correspond to the parameter x and the subsequent n_ϕ bits to parameter ϕ , followed by the binary representations for the α_i and β_i , $i = 2, \dots, n_s$ (see Figure 7).

Individuals are evaluated using the fitness function proposed by Gottwald et al.,¹⁰

$$f(\mathcal{I}) = \exp\left(1 - \frac{F(\mathcal{I})}{F_0}\right) \quad (14)$$

with $F(\mathcal{I})$ being the free energy per particle of the lattice structure represented by the individual \mathcal{I} . For a binary mixture at zero

(19) Fornleitner, J.; Lo Verso, F.; Kahl, G.; Likos, C. N. *Soft Matter* **2008**, *4*, 480.

temperature, this quantity is given by

$$F(\mathcal{T}) = \frac{1}{s} \left[\frac{n_A}{2} \sum_{ij} \Phi_{AA}(\mathbf{ia} + \mathbf{jb}) + \frac{n_B}{2} \sum_{ij} \Phi_{BB}(\mathbf{ia} + \mathbf{jb}) + \sum_{ij} \sum_{l=1}^{s-1} \sum_{m=l+1}^s \Phi_{\varepsilon(l)\varepsilon(m)}(\mathbf{ia} + \mathbf{jb} + \mathbf{B}_l - \mathbf{B}_m) \right] \quad (15)$$

The summations over i and j run over all integer values such that $|\mathbf{ia} + \mathbf{jb}|$ is smaller than a suitable chosen cutoff radius r_c , to be discussed below. F_0 in eq 14 is the lattice structure of a reference system, in our case a one-component hexagonal lattice of the large particles at the same number density as the structure represented by \mathcal{T} .

As a reproduction mechanism, we have decided to use instead of a simple one-point crossover process,^{10,11} the so-called random crossover technique, which is schematically presented in Figure 8. Here individuals of a given generation (“children”) are created from selected pairs of individuals of the preceding generation (“parents”) with the help of a random assembly vector \mathcal{A} : the reproduction process starts by filling the vector with an arbitrary sequence of bits. Then, two parent individuals, \mathcal{P}_0 and \mathcal{P}_1 , are selected according to their fitness values. The first child, \mathcal{C}_0 , is constructed bit by bit in the following way: the bit at position ν is taken from parent \mathcal{P}_0 (or \mathcal{P}_1) if the value of the bit at position ν in the assembly vector \mathcal{A} is 0 (or 1). Child \mathcal{C}_1 is generated from child \mathcal{C}_0 via simple bit-inversion.

Because of the finite number of bits used in the encoding of the parameters, the GA is not able to converge fully to the final solution. Additional refining mechanisms, for which we use a simple hill-climbing search,²⁰ are needed to relax the structure proposed by the GA. The result of this hill-climbing optimization represents the final solution of our search, i.e., the final MEC.

In order to guarantee a high reliability of our method, each state point (characterized by particle density $\eta\sigma_A^2$, concentration C , and particle size ratio z) is considered in a two-step process: First, several independent GA runs are performed with a cutoff radius r_c of considerable size (see below). These obtained structures and their respective energies are compared. The lattice with the overall lowest free energy is reconsidered in the second step, but now with an even larger cutoff radius. The structure that emerges from this search is then taken as the MEC for this particular state point. This rather high numerical effort might seem exaggerated at first sight, but we have good reasons for this strategy: the large number of parameters that characterizes a two-dimensional lattice leads to a rough energy landscape and the slowly decaying potential is responsible that the fitness function depends in a very sensitive way on the numerical parameters. Thus, GA runs carried out for one state point using a moderate cutoff radius do not necessarily converge to the same energetic minimum, which forces us to suitably adapt the numerical parameters (i.e., the mutation rate, the number of individuals per generation, etc.). Furthermore, performing identical runs provides additional information on the roughness of the energy landscape in the immediate surrounding of the found energy minimum and makes degenerate structures accessible.

We conclude this section by presenting explicit values for the numerical parameters that we have used: In every run we have generated 200 generations, consisting of 1000 individuals each. The mutation rate was set to $p_m = 0.01$. For the encoding step we

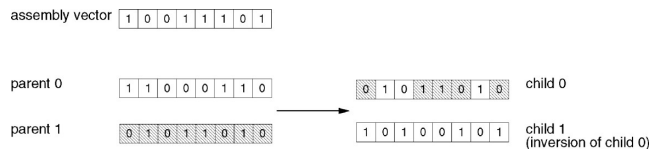


Figure 8. Schematic representation for a random crossover process.

use $n_p = 12$ for x , the α_i , and the β_i ; and $n_\phi = 6$; our numerical tests have given evidence that a larger number of genes does not increase the efficiency of the GA. Because of the slow decay in the interparticle potentials, we have used in the first search step outlined above a cutoff radius, $r_c = 200\sigma_A$ for the evaluation of the lattice sum. This value for r_c guarantees even at high densities that an increase of r_c by 10% leads to a relative change of the lattice sum of less than 0.01%. For the second step in our search strategy, i.e., for the overall best structure, a cutoff $r_c = 1500\sigma_A$ was used.

For practical reasons, we have limited the number of particles per unit-cell to $s = 8$, as the computational cost increases with the number of particles, and the GA search shows insufficient convergence if too many parameters are to be optimized. Thus we can investigate values for the concentrations of the smaller particles, $C = n_B/(n_A + n_B)$, in the range of $C = 1/8, \dots, 7/8$. In this way, for particular C values, we could perform independent GA runs for a given state point using unit-cells of different size: for instance, a system with $C = 1/2$ could be realized using 2, 4, 6, or 8 particles per cell. Finally, we have also included the case $C = 2/9$ (i.e., $s = 9$) in our investigations, since this particular ratio is known to give rise to special, highly asymmetric structures.¹⁵

4. Results and Discussion

In Figures 9–12 we present the MECs obtained with the GA-based search strategy described above by systematically varying the particle size ratio z and the concentration of small particles $C = n_B/(n_A + n_B)$ in our mixture of dipolar colloids. For clarity we show our results on four different panels: Figure 9 shows the structures for concentrations of small particles $C \leq 1/2$ and particle size ratios z ranging from 0.1 to 0.41. Figure 10 contains the structures for the missing size ratios up to $z = 0.9$ at the same concentrations of small particles. Figures 11 and 12 show the structures obtained for $C > 1/2$. All shown configurations are of a particle area density of $\eta\sigma^2 = 0.6$.

The main general trend to be observed for all investigated concentration rates is the system’s tendency to form lanes at large particle size ratios ($z \geq 0.5$; for examples, see especially Figure 12a–o). This inclination to stripe-like structures might indicate a region of phase separation, a phenomenon not directly accessible because of our search algorithm’s inherent restriction to periodic structures. At $z = 0.8$ and above, the difference between the two particle species is no longer pronounced enough to produce distinctive deviations from a uniform hexagonal lattice (see Figure 10m–t and Figure 12p–y; the different coloring of the particles can be misleading to the eye in this respect). Additionally, the GA experiences difficulties in finding the global energy minimum as the energy-landscape flattens out as a result of the potentials becoming increasingly alike. We will therefore exclude the results obtained for particle size ratios larger than $z = 0.7$ from the following discussion.

Results for $C \leq 1/2$. We start a more detailed discussion with the lattices obtained for $C \leq 1/2$, as their common features are easily visible. Changing the concentration of small particles

(20) Schwefel, H. P.; *Evolution and Optimum Seeking*; John Wiley and Sons: New York, 1995.

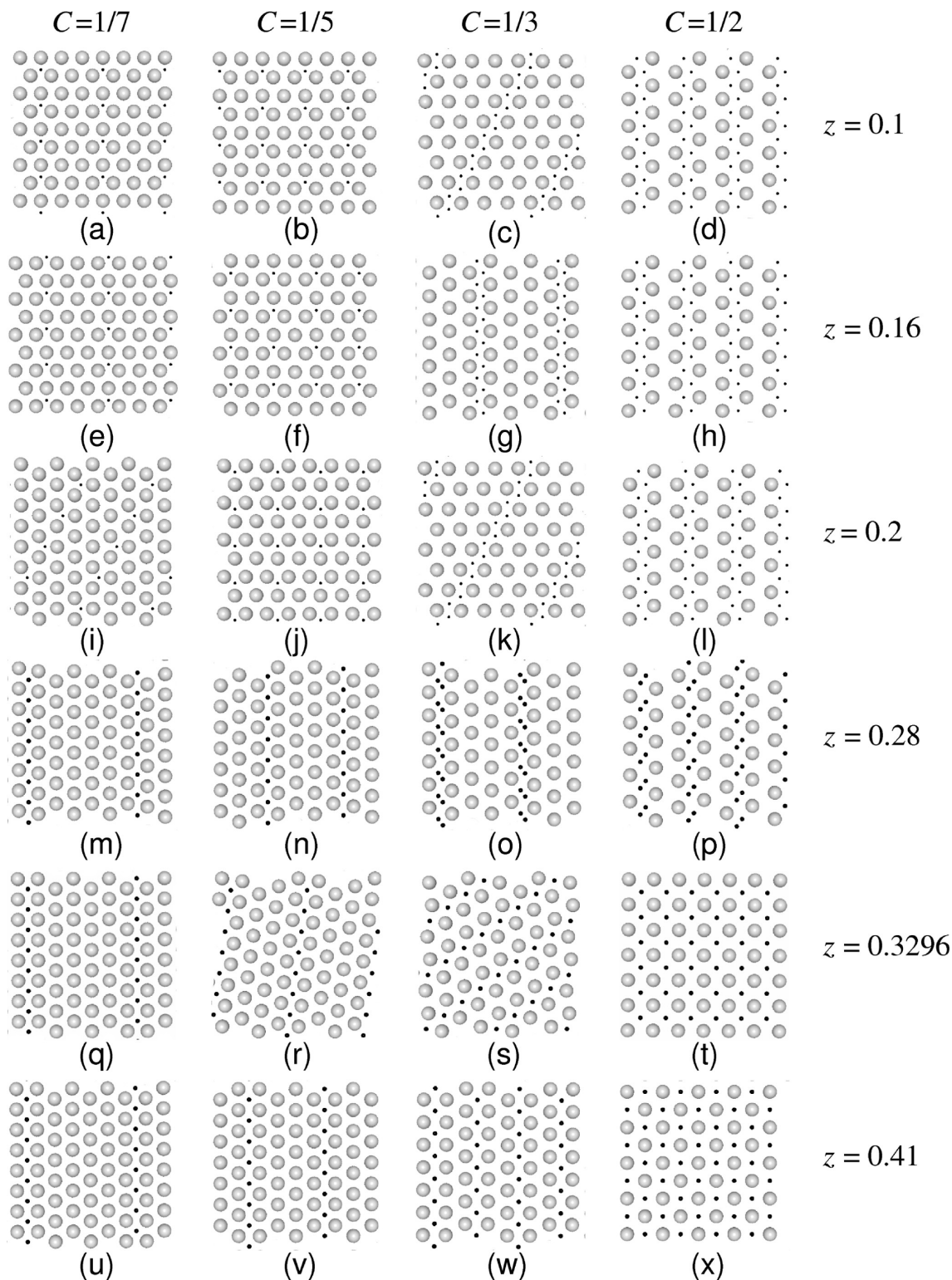


Figure 9. Found MECs for $C \leq 1/2$ and $z \leq 0.41$. The particles are not drawn to scale.

C results in changes of the size of the area occupied by a hexagonal lattice formed only by the large particles. The particle size ratio z , on the other hand, influences the form of the cage, the large particles build around the small ones: If z is small, the small particles are incorporated into the hexagonal lattice of the large ones without disturbing their immediate surrounding ($z = 0.1$ – 0.2 , see Figure 9a,b,e,f,i,j) so that they populate the centers of equilateral triangles of large particles. As z increases, the influence of the small particles on their

surrounding becomes more pronounced, and the triangles of large particles around the small ones are distorted; first to a rhomboid ($z = 0.28$, Figure 9m,n) and then to a square with the small particle sitting at the center ($z = 0.3296$ – 0.5 , Figure 9q–x and Figure 10a–d). Finally, the square cage of the large particles then deforms to a rectangle until it finally meets the requirements to fit into a hexagonal lattice, and, for $z \geq 0.8$, we arrive at the uniform case (see Figure 10, the rectangle is clearly visible in panels m, n, and q). In the case of $C = 1/3$ and $1/2$, an additional

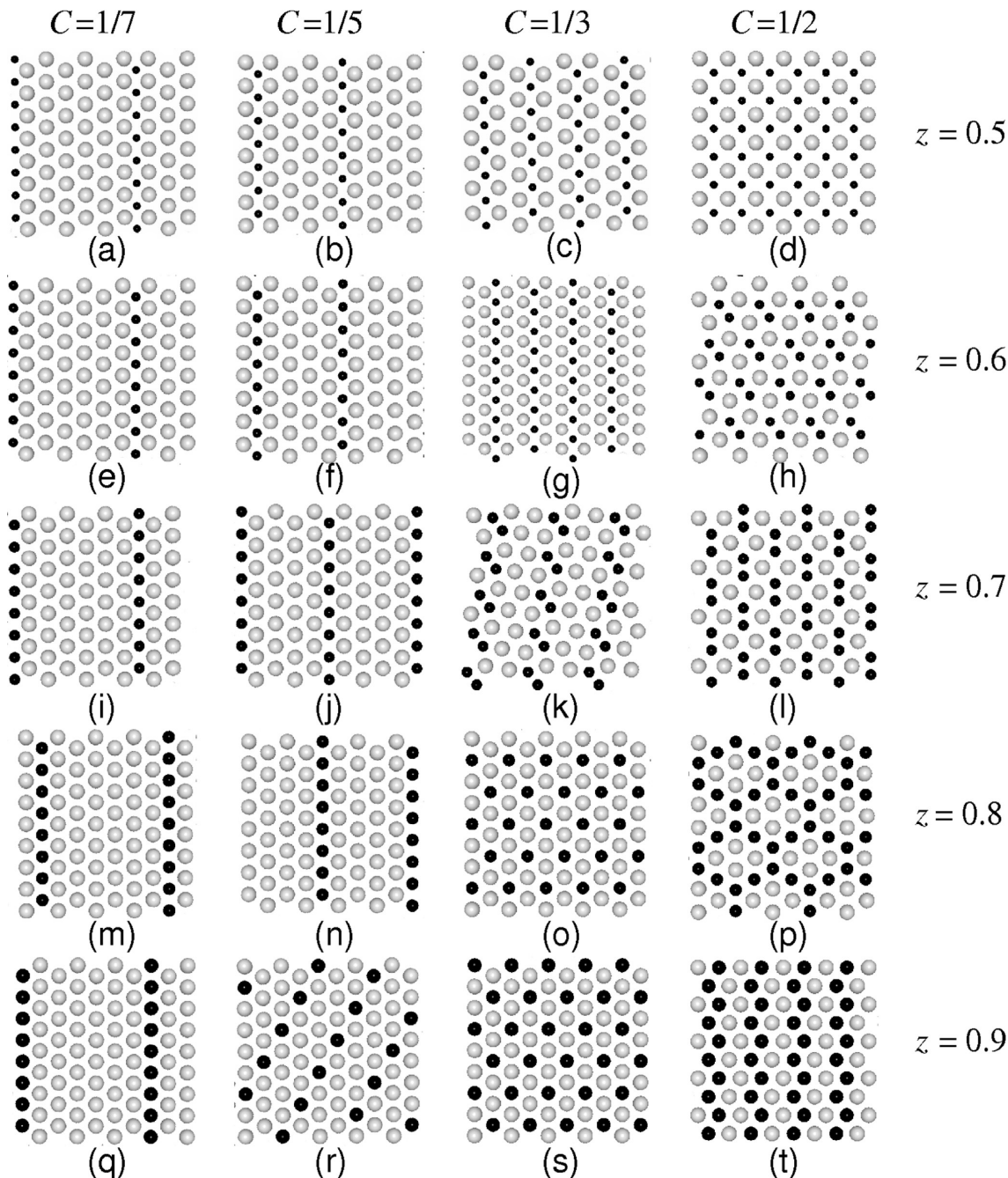


Figure 10. Found MECs for $C \leq 1/2$ and $z > 0.41$. The particles are not drawn to scale.

phase appears for small values of z ($z \leq 0.28$). The triangular cages arrange next to each other, and stripes of small particles, meandering through a slightly deformed hexagonal lattice of large ones, emerge. We believe that a similar ground-state for $C = 1/7$ and $1/5$ was inaccessible to our survey because of the limitation to a maximum of eight particles per cell.

It is pertinent to point out that all the various structures displayed in Figure 9 and Figure 10 consist of only a small number of different lattice elements or “tiles”: an equilateral triangle of large particles, with or without a small one in its center (see Figure 9a or b for example), a lozenge of large particles containing a pair of small ones, which is aligned along the longer diagonal (e.g., Figure 9d), a large rectangle or square around a small particle (e.g., Figure 10i or c), and an elongated hexagon with two small particles inside (Figure 10h,k,l). We believe that this occurrence of tiled phases might be an

indicator of so-called *random tiling* phases¹⁵ or even quasi-periodic structures; both scenarios are inaccessible to our search strategy.

Results for $C > 1/2$. General trends for mixtures with an abundance of small particles in the unit cell ($C > 1/2$) are harder to make out as the structures get more complex with increasing C , although common features can be identified: at the very low value of $z = 0.1$, the small particles tend to group into small clusters of various shapes, populating the interstitials of an ideal hexagonal lattice of the large particles. As z increases, the formerly distinct groups of small particles merge ($0.1 < z \leq 0.41$), until finally stripe-like structures emerge ($0.41 < z \leq 0.7$). We want to pay close attention to how these complex structures form by discussing the obtained sequences in more detail. Because of the small unit cell involved, the sequence at $C = 2/3$ clearly reflects the general trend: We start out with

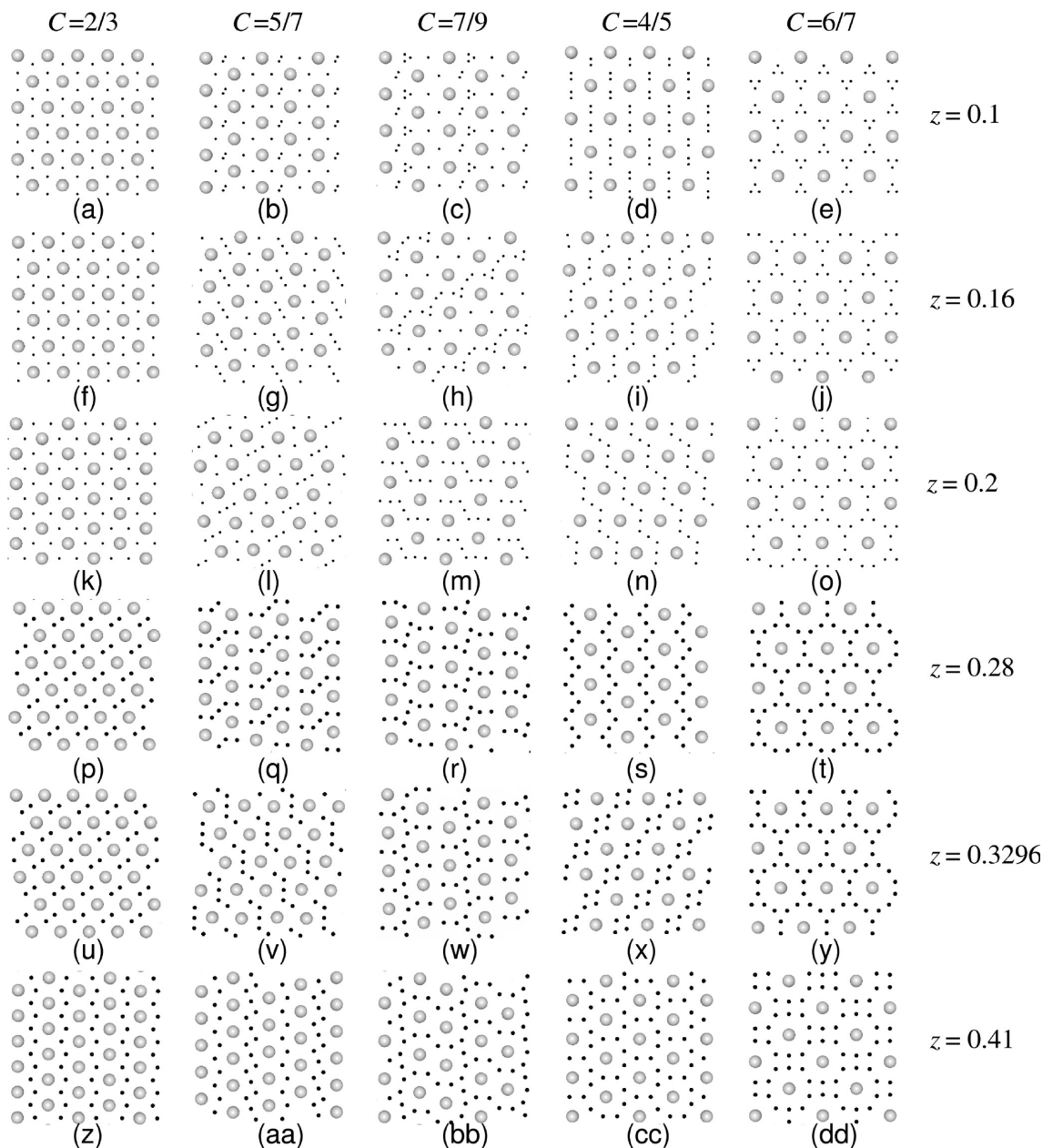


Figure 11. Found MECs for $C > 1/2$ and $z \leq 0.41$. The particles are not drawn to scale.

isolated single particles at the interstitials of the large particles' hexagonal lattice ($z = 0.1$ – 0.2 , Figure 11a,f,k). If they increase in size, two of them approach each other, first forming a distinct pair ($z = 0.28$ and 0.3296 , Figure 11p,u), and then, by a small change in the relative orientation of the originally parallel aligned dimers, pairs from adjacent cells combine to lanes ($z = 0.41$ – 0.6 , Figure 11z and Figure 12a,f). In the next case ($C = 5/7$), the obtained sequence is much more complex. At very small particle size ratios, we find dimers in addition to single small particles at the interstitials of the hexagonal lattice of large particles ($z = 0.1$, Figure 11b). Increasing their size lets one single particle join the adjacent dimer, and elongated trimers emerge for $z = 0.16$ and $z = 0.2$ (Figure 11g,l). With further increase of size, every trimer is joined by two more single particles to form zigzag-shaped pentamers ($z = 0.28$ and 0.3296 , Figure 11q,v), which, in turn, merge to form lanes ($z \geq 0.4$). As soon as neighboring pentamers are close enough to merge, they share the particles at their respective ends, and an additional, less populated lane of small particles springs up

($z = 0.41$, Figure 11aa). At size ratios from $z = 0.5$ to $z = 0.7$, rearrangements occur within the lanes, but the overall, stripe-like structure remains. For $C = 7/9$, we encounter cup-like structures, where every large particle is surrounded by a ring segment of small particles (see Figure 11r,w,bb for examples). The “cups” have their origin in the deformation of zigzag-shaped heptamers, formed at low particle size ratios ($z = 0.2$, Figure 11m): increasing z leads first to a deformation of the heptamers to arcs of small particles around a large one ($z = 0.28$, Figure 11r) and then to stripes of joint heptamers ($z = 0.3296$ and $z = 0.41$, Figure 11w,bb). At $z = 0.5$ and above, the cup-like features are no longer prominent, and we arrive at a normal, lane-like lattice. This occurrence of cups can be interpreted as a precursor of the formation of rings, encountered for the concentrations $C = 4/5$ and $C = 6/7$. For $C = 6/7$, the rings of small particles surrounding the positions of the large ones in a more or less ideal hexagonal lattice are already recognizable at very low values of z and remain stable over a long range of particle size ratios ($z = 0.1$ – 0.3296 , Figure 11e,j,o,t,y). The transition to the

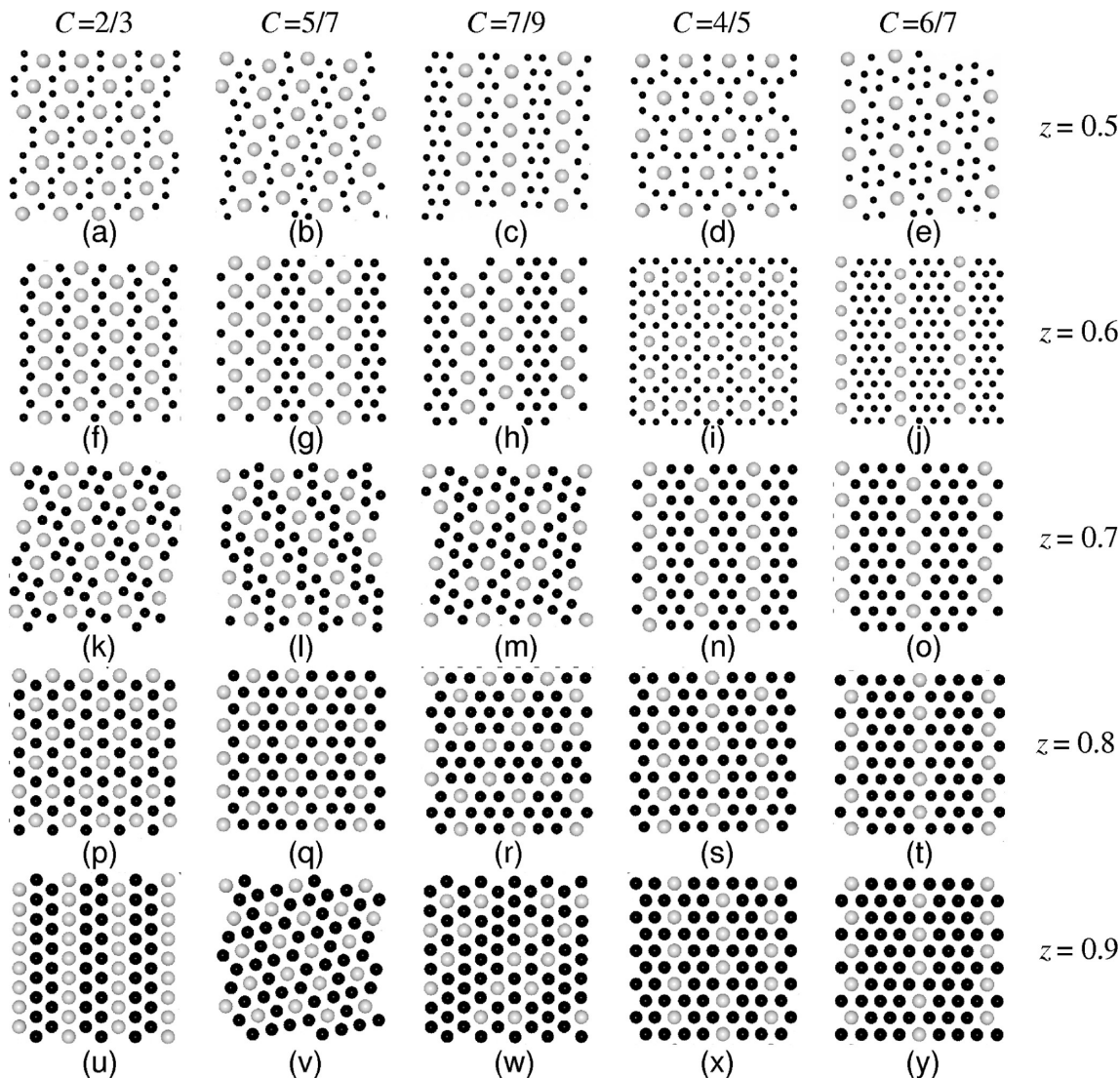


Figure 12. Found MECs for $C > 1/2$ and $z > 0.41$. The particles are not drawn to scale.

stripe-like phases takes place via a deformation of the underlying hexagonal lattice of the large particles ($z = 0.41$, Figure 11dd), to a nearly ideal square lattice at $z = 0.5$ (Figure 12e). This transformation is accompanied by a reduction of the number of small particles surrounding a large one from 12 ($z \leq 0.3296$), to 10 ($z = 0.41$), and finally to 9 at $z = 0.5$. At particle size ratios larger than $z = 0.5$, the system exhibits distinct stripes of large and small particles (see Figure 12j,o). In the other case, at $C = 4/5$, we also observe the formation of small particle rings ($z = 0.41$ – 0.6 , Figure 11dd and Figure 12d,i), but this time they are not visible from small particle size ratios on, but are preceded by a sequence of zigzag-shaped or pearl-necklace lanes ($z = 0.16$ – 0.3296). Like at $C = 6/7$, the number of small particles forming a ring also shrinks at this concentration as z increases, starting with nine particles at $z = 0.41$ and $z = 0.5$ and diminishing to eight particles per ring at $z = 0.6$. For even higher values of z , the stripe scenario is realized once more.

Comparison to a Hard-Disk Mixture. In an effort to understand the mechanisms leading to the observed MECs, we compare our findings to a phase diagram of hard discs.¹⁵ All of the ordered, periodic structures found to be stable for hard discs are also present in our current survey on dipolar colloids (see Figure 13). Almost all of these lattices were found at z -values around the structures' magic values z^* , for which all neighboring

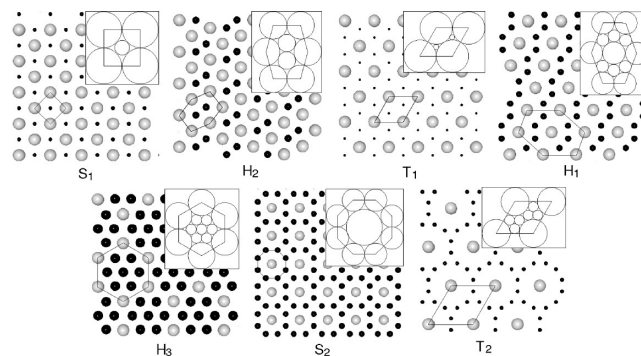
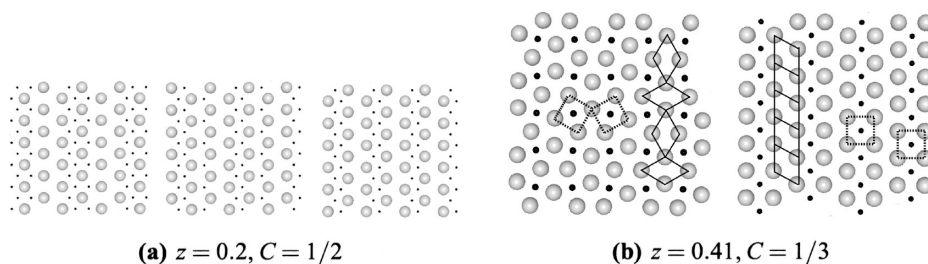


Figure 13. Equilibrium structures of the binary mixture (large pictures) with the corresponding stable lattices of the hard-disc system (small pictures). A possible choice of the unit cell is marked in both cases.

particles are in direct contact in the high-density, close packed unit cell. For the parameter sets made available by Likos and Henley¹⁵ and using the terms coined therein for the different lattices, we observe the following for the dipolar colloids: At $C = 1/2$, the S_1 -structure is obtained for $z = 0.3296$, 0.41 , and 0.5 , and the H_2 -structure is obtained for $z = 0.6$ and 0.7 . At $C = 2/3$, the dipolar mixture forms T_1 -like structures at

Table 1. Summary of Comparison between Dipolar Colloids and the Hard-Disc System

C	structure	z -values (dipolar colloids)	z -interval (hard discs) ^a	z^{*a}
1/2	S_1	0.3296, 0.41, 0.5	[0.392, 0.414]	0.414
1/2	H_2	0.6, 0.7	(0.414, 0.438] \cup [0.627, 0.646]	0.637
2/3	T_1	0.1, 0.16, 0.2, 0.28, 0.3296	[0, 0.312]	0.155, 0.281
2/3	H_1	0.41, 0.5, 0.6	[0.517, 0.546]	0.533
7/9	H_3	0.8	(0.101, 0.110] \cup [(0.378, 0.408]	0.386
4/5	S_2	0.3296, 0.6	(0.101, 0.123] \cup [0.193, 0.245]	0.216, 0.62
6/7	T_2	0.1, 0.16, 0.2, 0.28, 0.3296	[0, 0.157] \cup [0.315, 0.354]	0.101, 0.349

^a Reference 15.**Figure 14.** Two examples of degenerate structures (see text).

$z = 0.1-0.3296$ and H_1 -lattices at $z = 0.41-0.6$. An example of an H_3 -structure is found at $C = 7/9$, $z = 0.8$. S_2 occurs for $C = 4/5$, $z = 0.6$, and, for $C = 6/7$, we encounter T_2 -structures in the range of $z = 0.1-0.3296$. (See Table 1 for a summary).

Most differences in regard to z occur because our method of investigation does not allow for nonperiodic lattices like *lattice gas phases*, where the small species can distribute randomly on the interstitial sites of the hexagonal lattice formed by the large particles, or *random tiling phases*, or the possibility of a phase separation; all phenomena that were included in the survey of Likos and Henley.¹⁵ Nonetheless, there are also cases in which the mixture of dipolar colloids shows behavior undiscovered in the hard-disc system: For low and intermediate values of z , the H_3 -structure ($C = 7/9$) is stable in the case of hard discs.¹⁵ The dipolar mixture shows distinctly different lattices throughout the whole range of particle size ratios (see Figure 11c,h,m,r,bb), all of which were explicitly checked against the H_3 -structure and proved to be of lower energy. At $C = 4/5$, instead of the S_2 structure occurring for hard discs, the dipolar mixture shows two different structures at low z , both unique to the system: A hexagonal lattice of large particles with small dimers sitting at the interstitials (Figure 11d) and zigzag-shaped lanes of small particles running through a hexagonal lattice of large particles (Figure 11i).

Degenerate Structures. The method of investigation as introduced at the end of section 3 allows us to identify degenerate structures, i.e., configurations that differ in the arrangement of particles while corresponding to the same (minimal) value of the free energy. As the numerical accuracy of our investigation procedure is mainly determined by the chosen cutoff radius in the calculation of the free energy, we define two structures to be energetically degenerate if the difference in their free energies per particle, ΔF , is of the same order of magnitude as the error due to the employment of a finite cutoff, i.e., if $\Delta F \lesssim 10^{-6} E_1$, with A referring to the energy scale of the system (cf. eqs 3–5).

We find degenerate structures at about a tenth of all the state points investigated. As long as z is small, the encountered degenerate phases exhibit the behavior of a lattice gas:¹⁵ the energetically equivalent structures differ only in the positioning of the small particles in the otherwise unchanged, hexagonal

host lattice formed by the larger species. Figure 14a shows a 3-fold degenerate structure found at $C = 1/2$, $z = 0.2$, displaying the mentioned characteristics. In addition to the lattice gas phase observed only at small values of the particle size ratio, we also encounter degenerate structures that consist of the same set of tiles, thus indicating the occurrence of random tilings. In Figure 14b, we present an example of degenerate tilings encountered for $C = 1/3$, $z = 0.41$, where squares of large particles hosting a small one at its center and empty rhombic unit cells of large particles arrange in two different patterns: in the first case, the rhombic cells align parallel to each other, establishing a distinct pattern of alternating lanes. In the other case, the orientation of the tiles changes along each lane, obscuring the pattern. Square and rhombic unit cells have been highlighted in Figure 14b, to enhance the visibility of the lane-like arrangement.

5. Conclusions

We have demonstrated that binary, isotropic, dipolar monolayers can order in an enormous variety of structures, which can be influenced by the mixture composition as well as the polarizability ratio between the particles. High asymmetries between the latter lead to intricate and highly nontrivial structures, unanticipated by conventional methods, a fact that underlines the power of GAs to perform efficient searches of the parameter space.

Our results should be readily verifiable in the appropriate experimental systems. However, it must be stressed that most likely the dynamics of crystal growth will come in the way of the development of sufficiently extended crystals in real systems. Indeed, as crystallites with random orientations will start growing at uncorrelated nucleation centers in the system, further growth is likely to be arrested either because of the mismatch between the grain boundaries or because of the intervention of glassy states. These problems are exacerbated by the highly nontrivial structure of the resulting alloys, which requires well-coordinated particle rearrangements even within a single, periodically repeating cell. One possibility to circumvent this difficulty experimentally is to employ external fields that are *tilted* with respect to the confining plane. This strategy induces a preferred direction along which crystallites grow, namely the one dictated by the in-plane projection of the external field, which reduces the repulsions or even

induces attractions for sufficiently high tilt angles. Admittedly, the alloys resulting in such anisotropic situations will be different than the ones discovered here, as confirmed by ongoing research on this topic.²¹ However, it might prove advantageous to *first* tilt the field, so as to grow a sufficiently extended crystal and *then* slowly reduce the tilt angle back to zero, allowing for the now periodically ordered particles to reach their new equilibrium positions.

Finally, we point out that considerable interest has been raised recently on the possibility to tune the phononic spectra of soft materials through tuning of their interactions and the resulting crystal structures,^{22,23} including the possibility of employing confining laser-fields.²⁴ Binary compounds, such as those described in our work, open up another way to this goal, since the complex geometry and high number of basis particles in a unit cell

(21) Chremos, A.; Likos, C. N. In preparation.

(22) Cheng, W.; Wang, J. J.; Jonas, U.; Fytas, G.; Stefanou, N. *Nat. Mater.* **2006**, *5*, 830.

(23) Baumgartl, J.; Dietrich, J.; Dobnikar, J.; Bechinger, C.; von Grünberg, H. *H. Sofi Matter* **2008**, *4*, 2199.

(24) Baumgartl, J.; Zvyagolskaya, M.; Bechinger, C. *Phys. Rev. Lett.* **2007**, *99*, 205503; **2008**, *100*, 219903(E).

will give rise to a number of corresponding optical branches in the phonon spectra. Tuning of the composition and mass ratio readily allows us then to steer the width and number of associated phononic gaps in the material. Results on this topic will be the subject of a future publication.²⁵

Acknowledgment. C.N.L. wishes to thank the Erwin Schrödinger International Institute for Mathematical Physics (ESI, Vienna), where parts of this work have been conducted, for a Senior Research Fellowship and for its hospitality. This work has been supported by the Austrian Research Foundation (FWF), project number P17823-N08, the European Science Foundation short-visit-grants “SimBioMa 1730” and “COST-STSM-P13-015” (J.F.), by the Marie Curie program of the European Union, contract number MRTN-CT2003-504712 and the Foundation Blanceflor Boncompagni-Ludovisi, née Bildt (F.L.V.), as well as by the DFG within the SFB-TR6, Project Section C3.

(25) Fornleitner, J.; Kahl, G.; Likos, C. N. In preparation.